Supplement of SOIL, 12, 421–440, 2026
https://doi.org/10.5194/soil-12-421-2026-supplement

Supplement of

Weathering without realizing inorganic CO_2 removal revealed through base cation monitoring

Arthur Vienne et al.

Correspondence to: Arthur Vienne (arthur.vienne@uantwerpen.be) and Sara Vicca (sara.vicca@uantwerpen.be)

Overview of Supplementary data

S1 Environmental variables: temperature, soil moisture, water inputs, leaching volumes
S2 Rock characterization: Particle size distribution, XRD, XRF and BET-SSA
S3 Additional Data

S1 Environmental variables

S1.1 Temperature

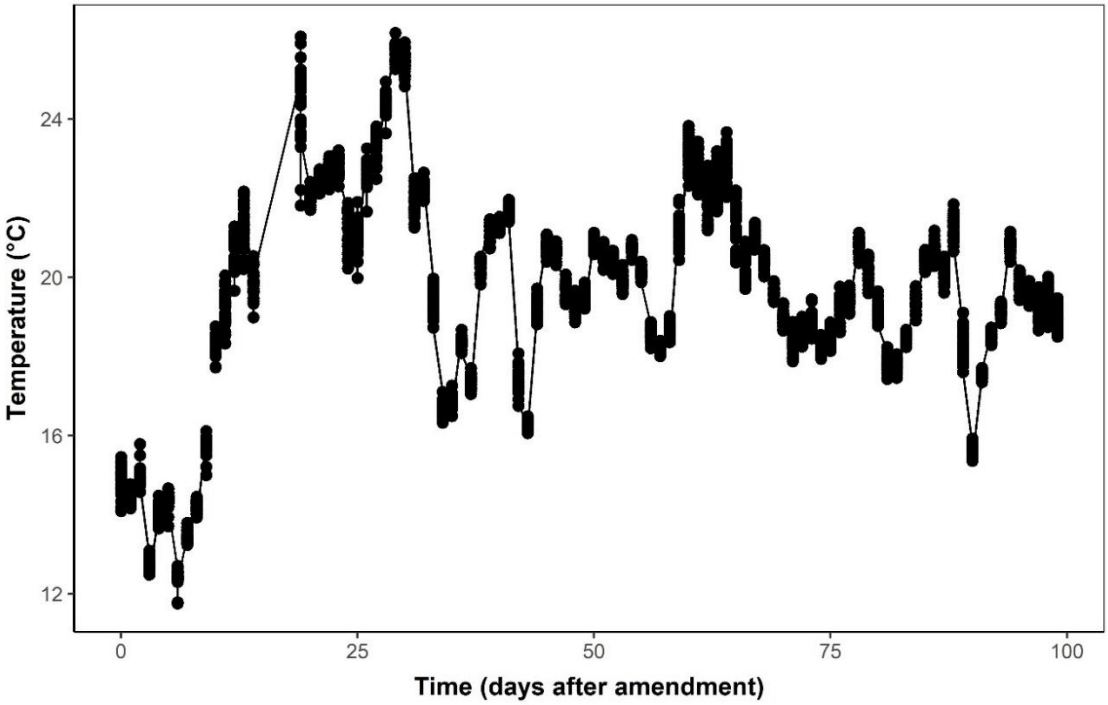

Fig. S1: Soil temperature fluctuations over time.

S1.2 Water inputs

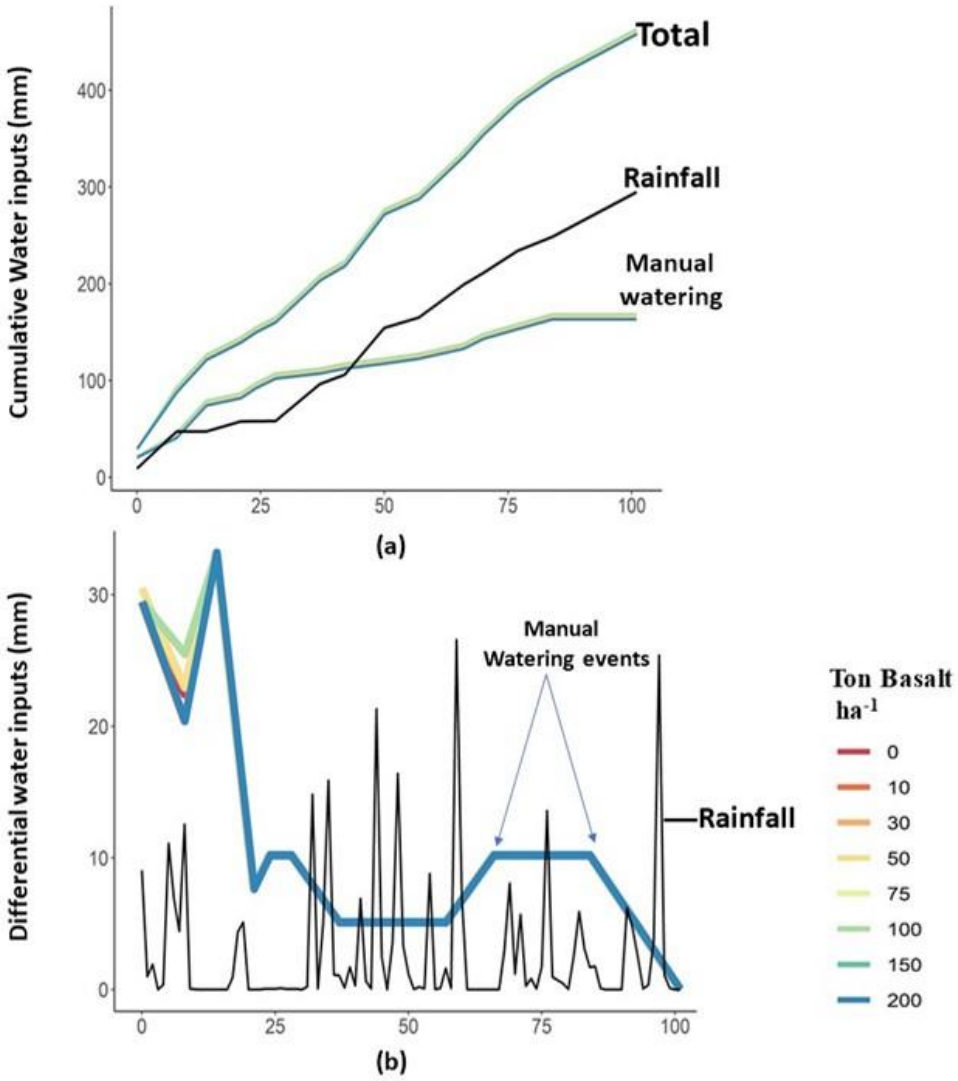

Fig. S2: (a) Cumulative (mm) and (b) daily water inputs (mm/day) in function of time after amendment (days). Note that water inputs were intended to be equal for all treatments, however due to a watering error around day 10, slightly different water inputs were given to some mesocosms. Cumulatively, the impact of this watering error was minor as illustrated for the range of basalt mesocosms in this figure.

S1.3 Soil moisture

Differences in soil water content were generally small between treatments and application rate. Nonetheless, all mesocosms became slightly drier after amendment. From Supplementary Figure 3, we derive graphically that for all added rock powders, roughly 80% of the particles are in the sand fraction, while control soil has only about 60% sand. The relative increase in sand fraction in amended soils is thus thought to lower SWC with higher basalt application. For Basalt, we observe a positive time x application rate interaction effect. Due to non-linearity of residuals of the lmer model, we opted to model SWC changes with a generalized additive model (GAM) with time as a smoother. The model outcome is summarized in **Table S1**.

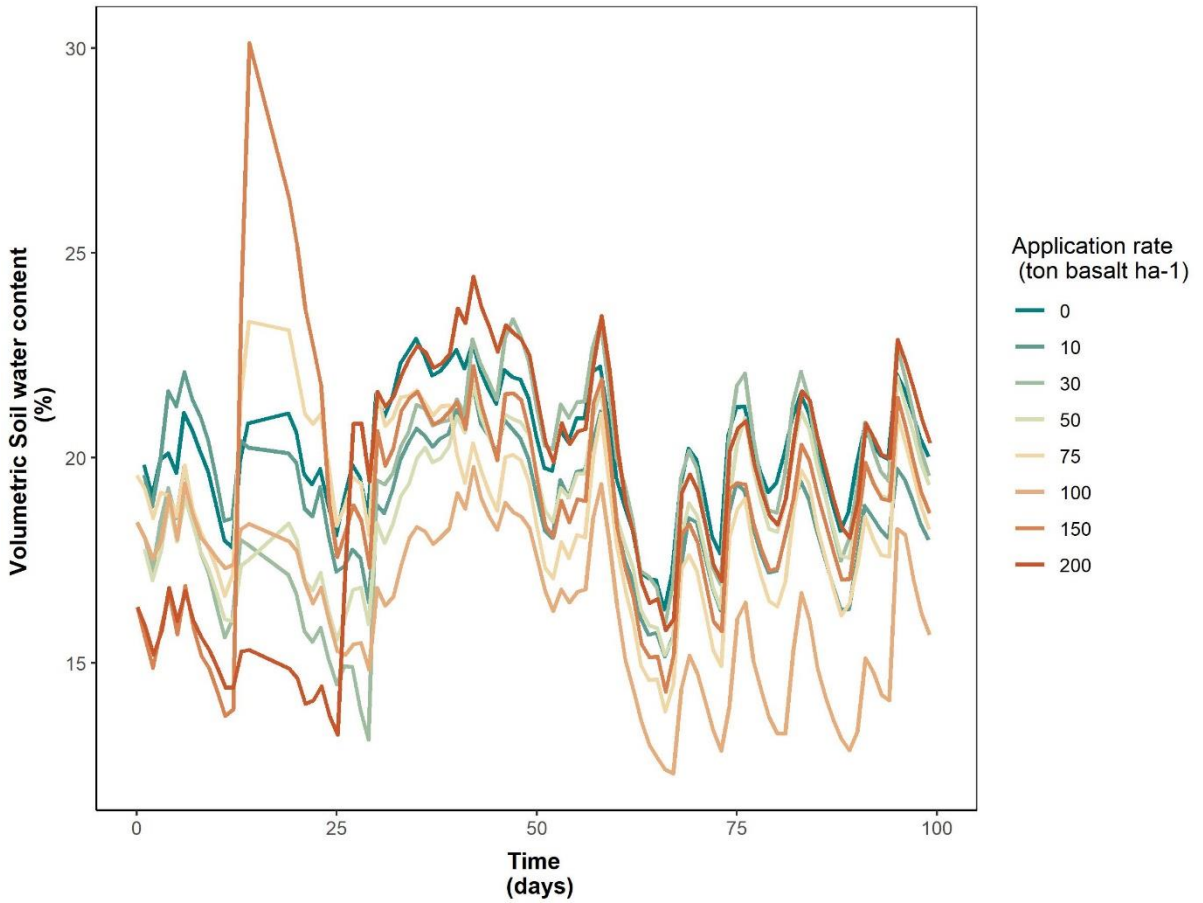

Fig. S3: SWC in function of time (days).

Table S1: Outcome of the GAMs for daily SWC data.

Silicate	delta SWC / (ton rock /ha)	Time effect (delta SWC / ton rock/ha/day)	Predicted difference in SWC with control soil for highest application rate (after 100 days)
Basalt	-1.29 e-4 (p <0.01)	+9.06 e-7 (p=0.05*)	-0.008

S1.4 leaching volumes

No significant differences in leachate volumes were observed within this experiment.

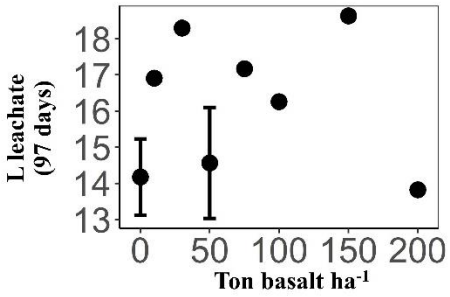

Fig. S4: Endpoints of cumulative leaching volumes (L/mesocosm) after 97 days in function of basalt application rate.

S2 Rock characterization: Particle size distribution, XRD, XRF and BET-SSA

Table S2: XRF of the applied DURUBAS basalt.

Durubas Basalt (DURUBAS data sheet)	
Element	Concentration (wt%)
SiO2	44.6
Fe2O3	11.7
CaO	10.8
MgO	12.9
Al2O3	11.5
Na20	2.6
TiO2	2.3
K2O	0.7
P2O5	0.9
MnO	0.2

Table S3: XRD and BET-SSA of the applied Durubas basalt.

Mineral phase (chemical formula)	**Mass %**
Clinopyroxene	21.22
Enstatite	0.66
Pigeonite	2.36
Forsterite	14.45
Hedenbergite	6.98
Ankerite	0.18
Grossmanite	1.29
Albite	1.29
Labradorite	5.7
Analcime	0.93
Quartz	0.07
Magnetite	2.73
Amorphous phase	42.14
BET-SSA	**9.226 ± 0.08 $m^2 g^{-1}$**

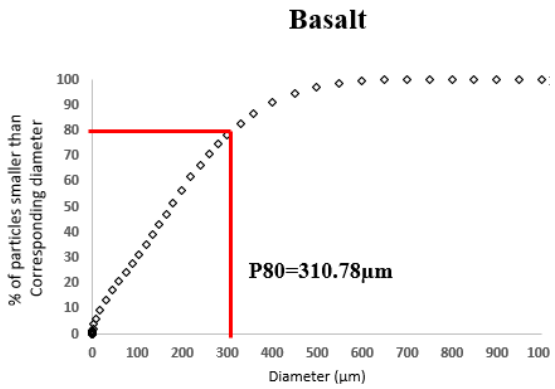

Fig. S5: PSD of the basalt rock powder.

S3 Additional data

S3.1 Soil water chemistry (topsoil pore water and leachates)

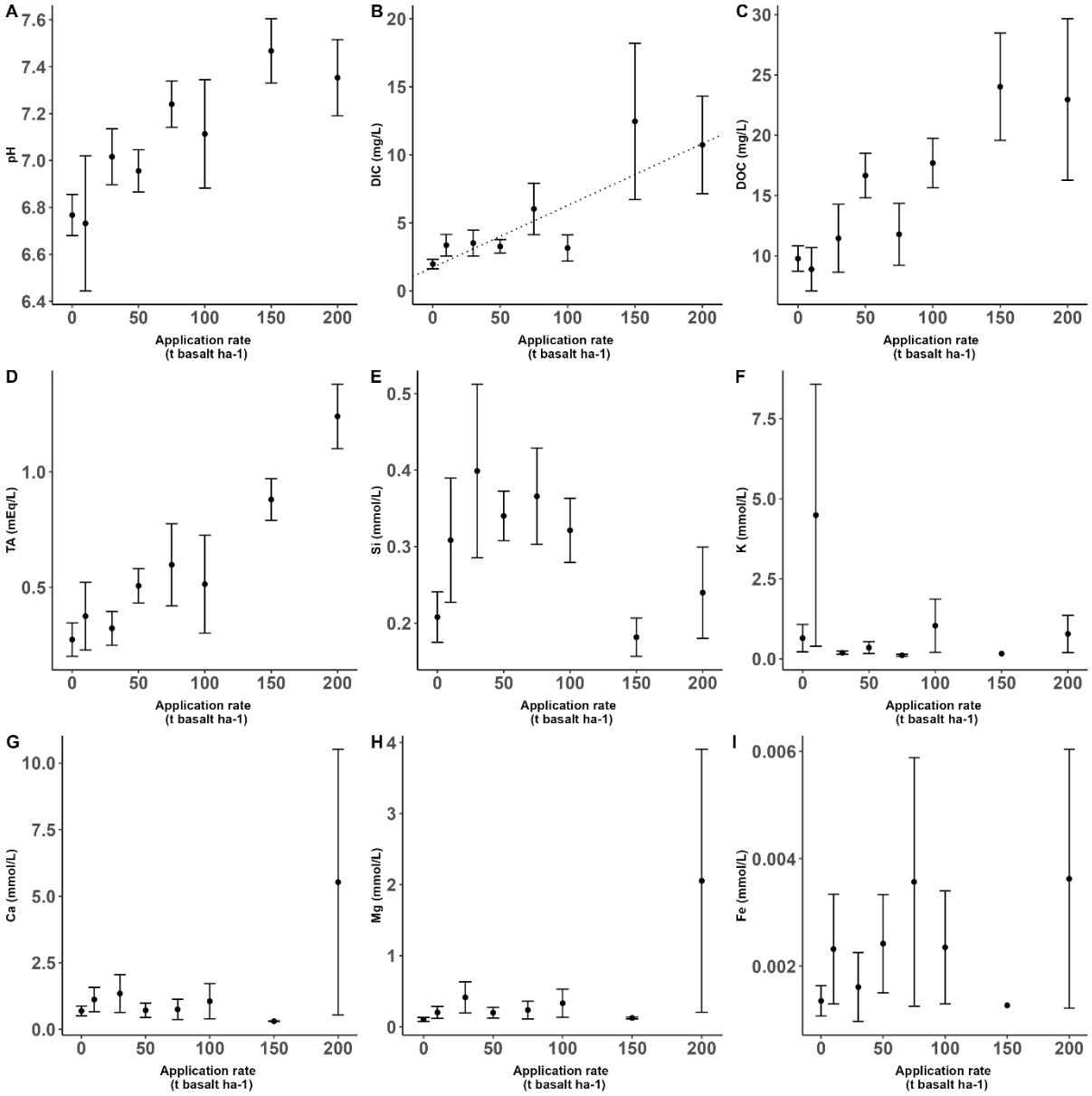

Fig. S6: Topsoil pore water chemistry at 10 cm depth in function of basalt application rate (a) pH (b) DIC (c) DOC (d) TA (e) Si (f) K (g) Ca (h) Mg and (i) Fe. Dots and error bars represent averages +- standard errors of all data collected during the experiment. n= 5 for control and the 50 t basalt ha-1 replicates at every moment of measuring if enough soil water could be sampled.

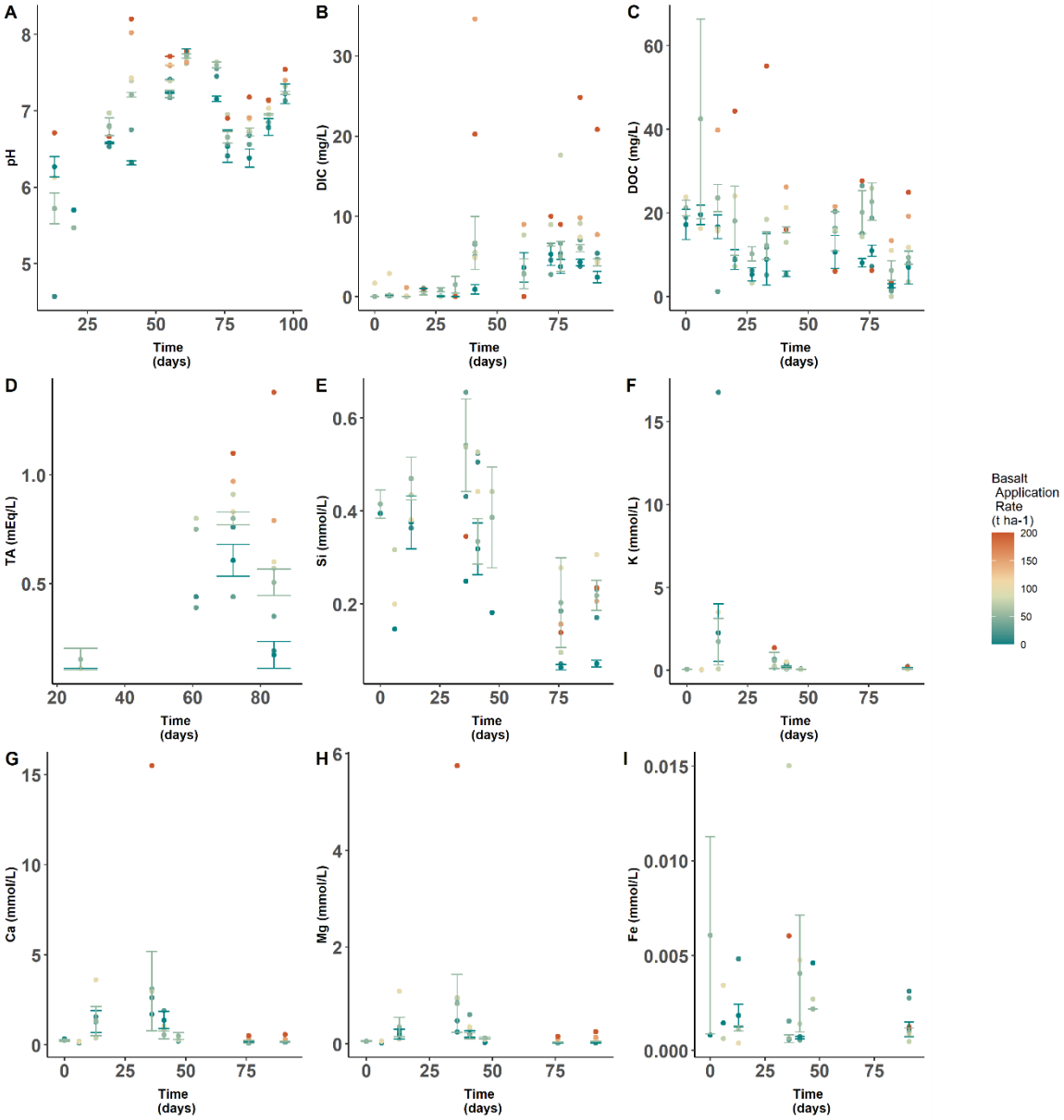

Fig. S7: Temporal dynamics of topsoil pore water chemistry at 10 cm depth for (a) pH (b) DIC (c) DOC (d) TA (e) Si (f) K (g) Ca (h) Mg and (i) Fe. n= 5 for control and the 50 t basalt ha-1 replicates at every moment of measuring if enough soil water could be sampled.

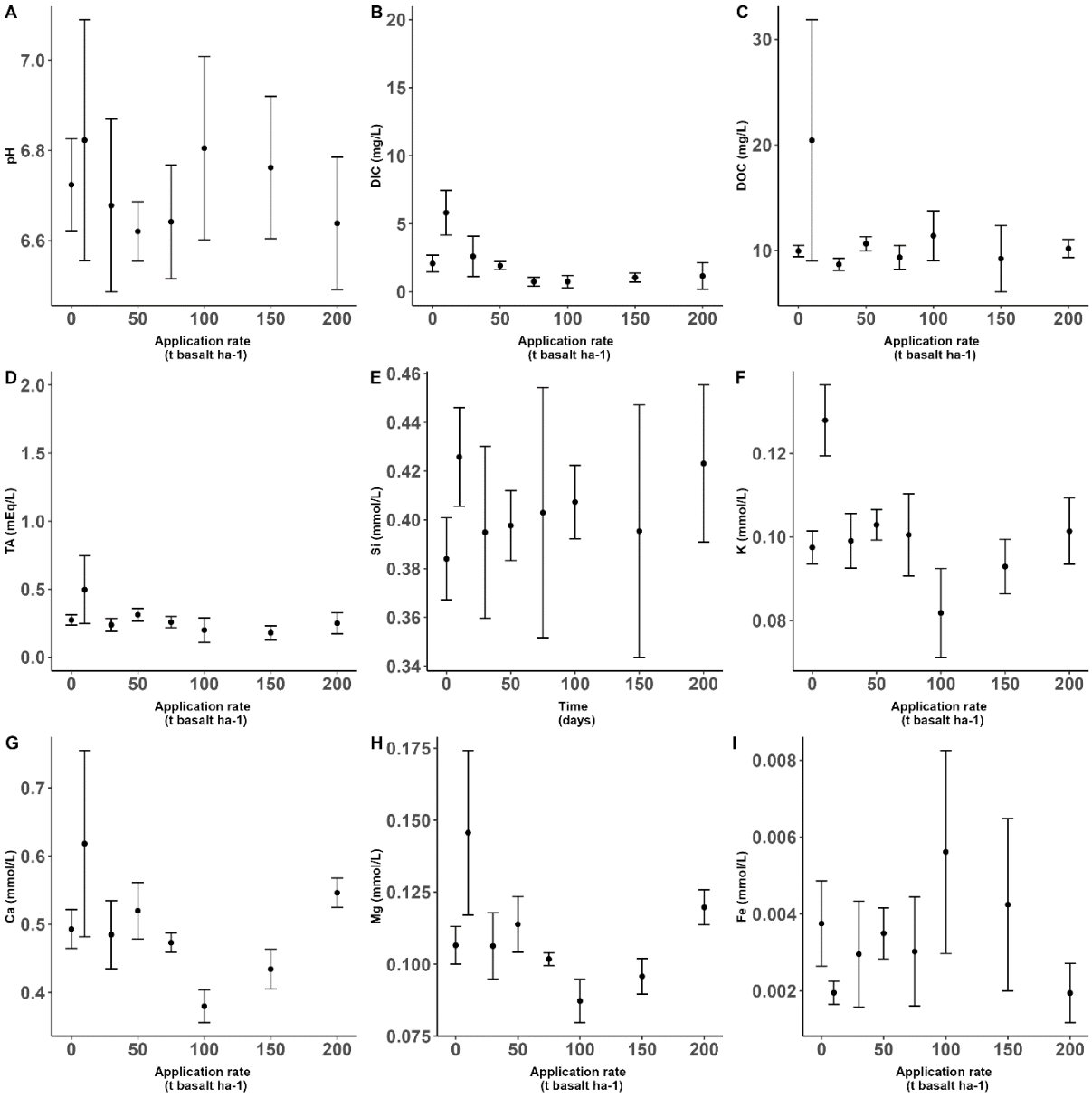

Fig. S8: Leaching water chemistry at 60 cm depth in function of basalt application rate for (a) pH (b) DIC (c) DOC (d) TA (e) Si (f) K (g) Ca (h) Mg and (i) Fe. Dots and error bars represent averages +- standard errors of all data collected during the experiment. n= 5 for control and the 50 t basalt ha-1 replicates at every moment of measuring if enough soil water could be sampled.

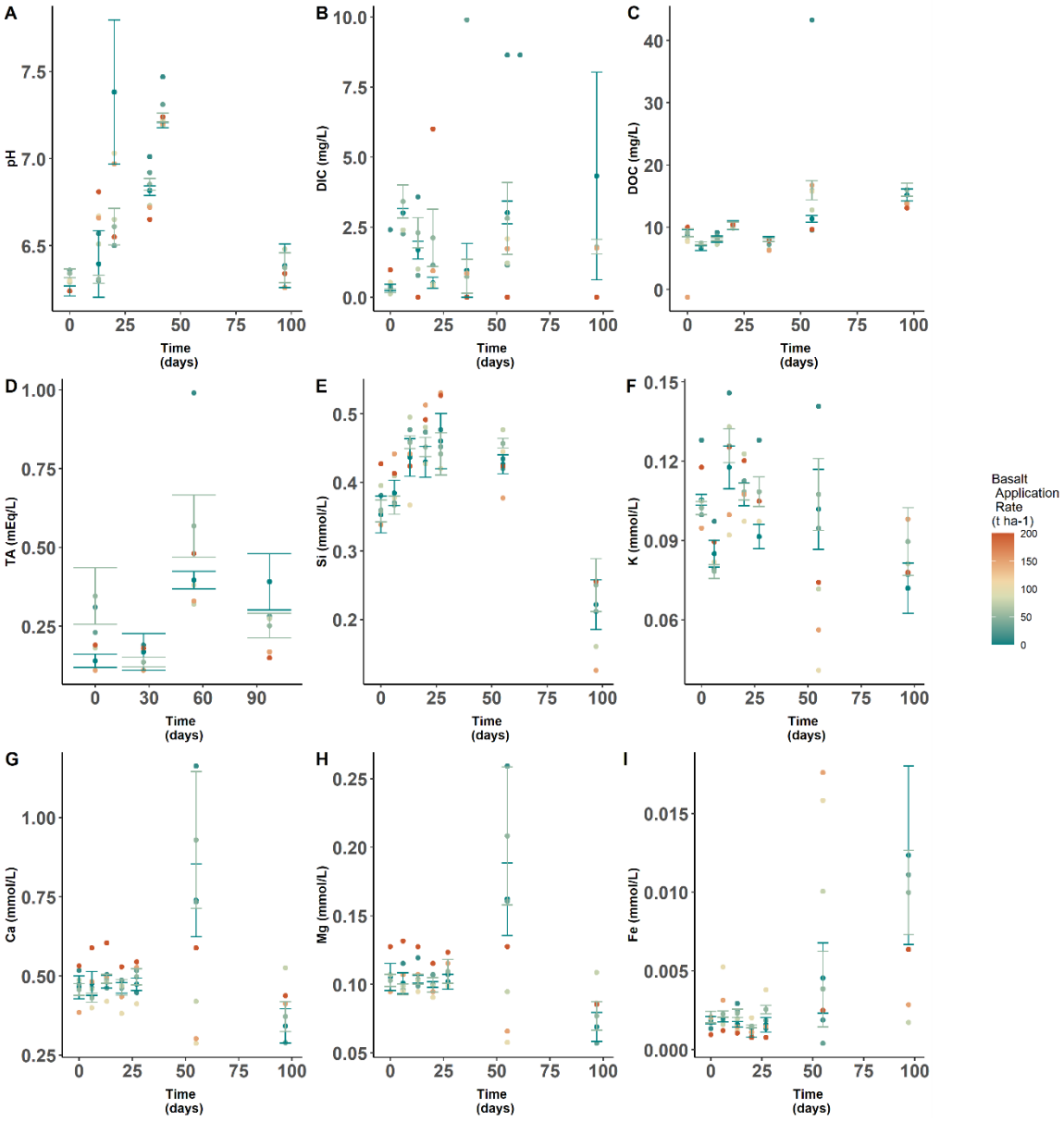

Fig. S9: Temporal dynamics of leaching water chemistry at 60 cm depth for (a) pH (b) DIC (c) DOC (d) TA (e) Si (f) K (g) Ca (h) Mg and (i) Fe. n= 5 for control and the 50 t basalt ha-1 replicates at every moment of measuring if enough soil water could be sampled.

Table S4: Effects and significance of effects of basalt amendment on different parameters in soil water in top soil (0-10 cm) and leachate water. Significant effects are indicated in bolt. N.S. = Not significant, interaction term was left out of the model.

Top soil pore water (0-10 cm)		
Parameter (unit)	Basalt effect and p-value	Time x basalt interaction effect and p-value
pH (-)	**+6.9 e-3 (p<0.01)**	**N.S.**
DIC (mg/L)	**+1.6 e-2 (p=0.27)**	**+4.9 e-4 (p=0.04)**

DOC (mg/L)	**+1.4 e-1 (p<0.01)**	**-1.21 e-3 (p=0.02)**
TA (mEq/L)	**+3.9 e-3 (p<0.01)**	**N.S.**
Si (mg/L)	+1.5 e-2 (p=0.09)	N.S.
K (mg/L)	-1.3 e-1 (p=0.64)	N.S.
Ca (mg/L)	**+1.7 (p<0.01)**	**-1.8 e-2 (p<0.01)**
Mg (mg/L)	**+4.3 e-1 (p<0.01)**	**-4.5 e-3 (p<0.01)**
Fe (mg/L)	+6.9 e-4 (p=0.16)	N.S.
Effluent water		
pH (-)	-2.2 e-4 (p=0.78)	N.S.
DIC (mg/L)	-9.1 e-3 (p=0.06)	N.S.
DOC (mg/L)	-7.7 e-3 (p=0.33)	N.S.
TA (mEq/L)	-4.5 e-4 (p=0.28)	N.S.
Si (mg/L)	+3.6 e-3 (p=0.34)	N.S.
K (mg/L)	-1.1 e-3 (p=0.43)	N.S.
Ca (mg/L)	-5.0 e-3 (p=0.70)	N.S.
Mg (mg/L)	-5.6 e-4 (p=0.76)	N.S.
Fe (mg/L)	-9.3 e-5 (p=0.81)	N.S.

S3.2 Method comparison: DIC, alkalinity and conductivity

Starting from 19/7/2021 electrical conductivity was also measured in the same water samples for carbon analysis using a 914 pH/Conductometer (Metrohm, Herisau, Switzerland) and a correlation curve between DIC and conductivity was constructed to investigate this relationship.

We find that DIC was correlated with specific conductivity (at 25°C), but a better correlation was found with measured total alkalinity (TA). Both conductivity and TA significantly correlated with DIC (both p <0.01). In correspondence with adjusted R^2 was however higher for TA (0.68) than for conductivity (0.45).

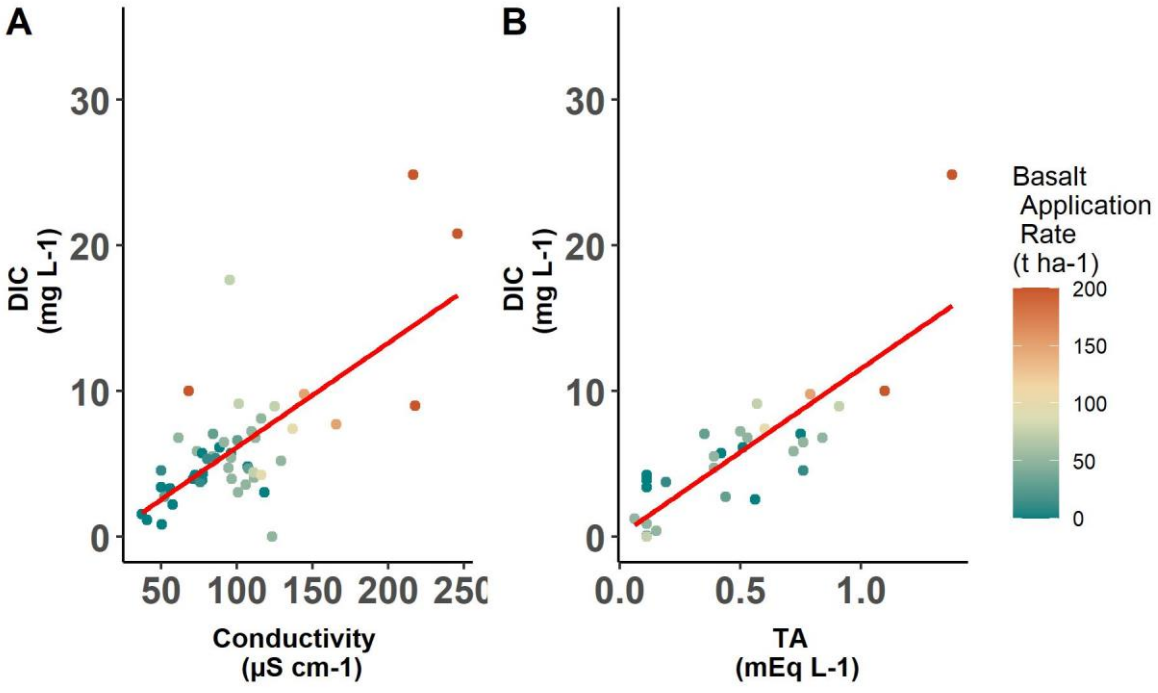

Fig. S10: Callibration curve between DIC and (A) electric conductivity (corrected to 25°C) and (B) total alkalinity. Red lines represent regressions.

S3.3 Results of sequential extractions for lower depths

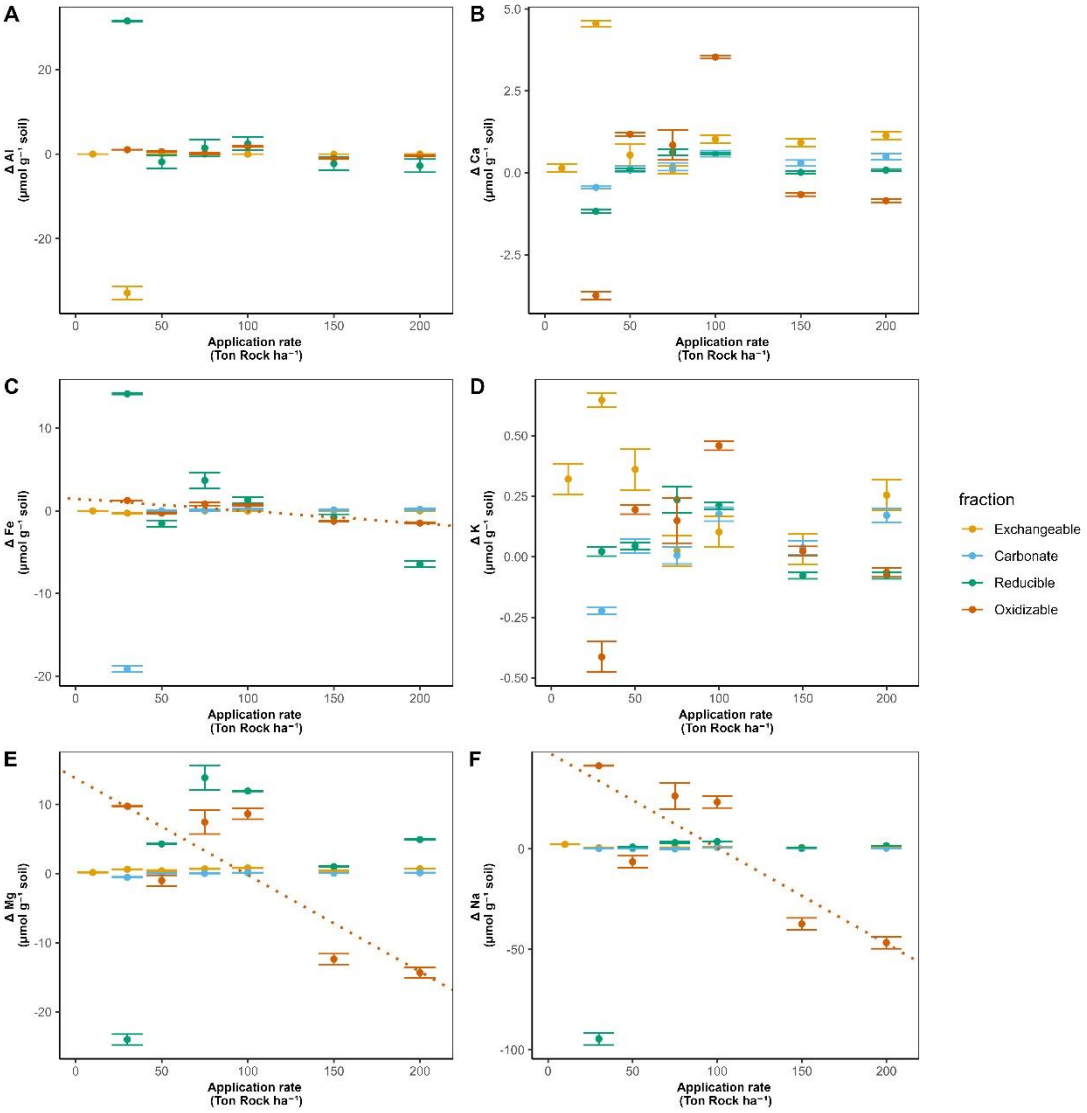

Fig. S11: Change in soil (20-30 cm) elements relative to control soils 100 days after basalt amendment, in function of rock application rate for (A) Al (B) Ca (C) Fe (D) K (E) Mg and (F) Na in four different soil pools. Dots and error bars represent averages and standard errors. n = 4 for control and 50 t ha^{-1} replication. Significant effects ($p<0.05$) of basalt application rate on cation concentrations are indicated with dotted lines. Note that y-axes absolute values differ for subplots to visualize smaller changes for certain elements.

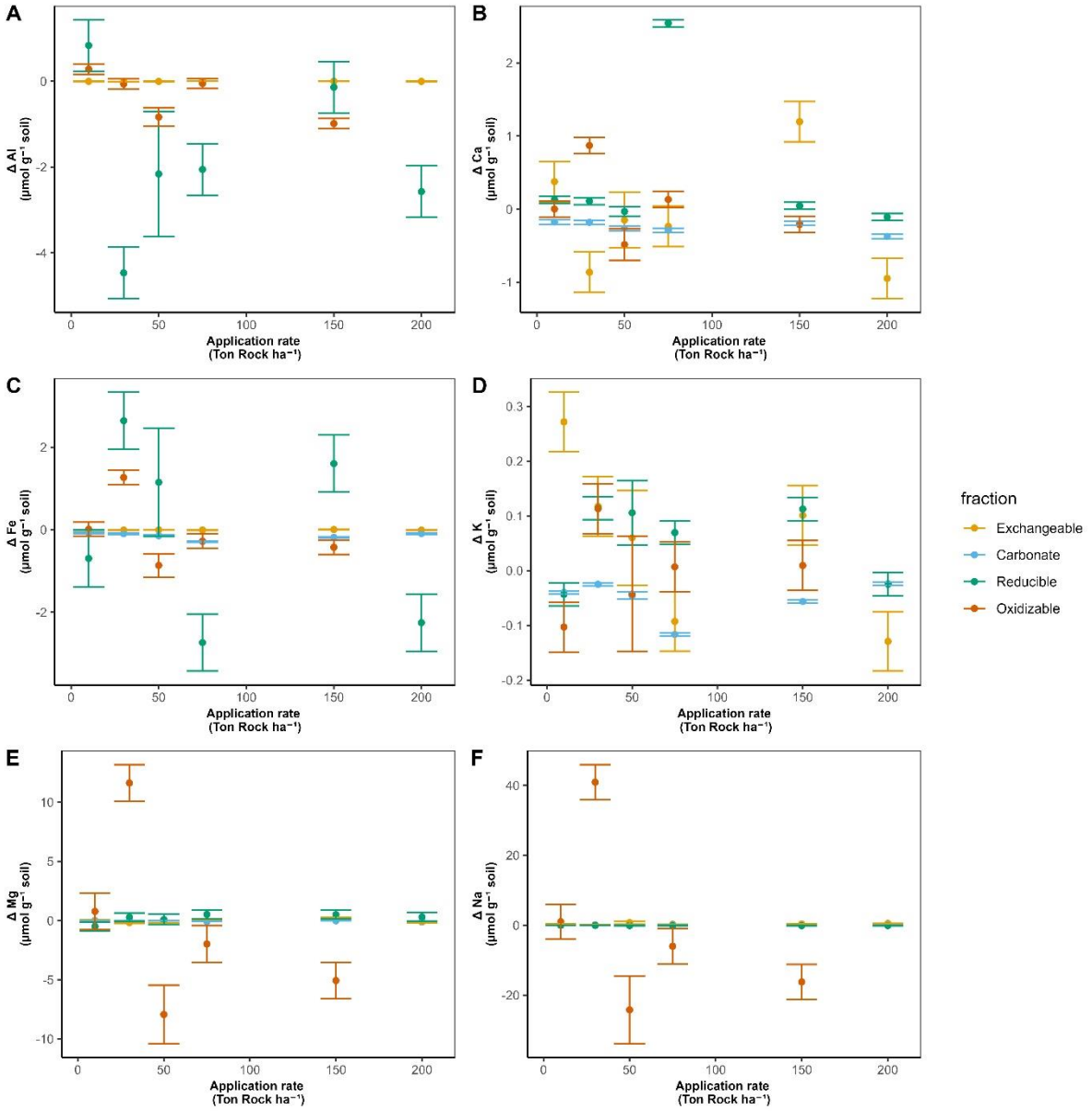

Fig. S12: Change in soil (30-50 cm) elements relative to control soils 100 days after basalt amendment, in function of rock application rate for (A) Al (B) Ca (C) Fe (D) K (E) Mg and (F) Na in four different soil pools. Dots and error bars represent averages and standard errors. n = 4 for control and 50 t ha^{-1} replication. Significant effects ($p<0.05$) of basalt application rate on cation concentrations are indicated with dotted lines. Note that y-axes absolute values differ for subplots to visualize smaller changes for certain elements.

S3.4 sensitivity analysis of weathering rates and base cation changes in (soil) pools

To assess the robustness of our regression approach that excludes data from certain application rates due to analytical errors in samples taken at certain depths for certain fractions, we also calculated the weathering rate for each application rate if possible (if a datapoint for every depth and soil pool was available and analytical errors did not occur). Due to analytical errors in at least one depth and soil pool for the the 10, 100 and 200 t ha-1 application rates (more specifically, errors occurred for the 20-30 cm 10 ton basalt ha-1 application rate and for the 30-50 cm samples in the 100 and 200 ton basalt ha-1 applications), we could not calculate an aggregated Wr for these application rates.

For the other weathering rates (30, 50, 75 and 150 t basalt ha-1), we subtracted TA equivalents in soil pools after basalt amendment from the mean control soil value and propagated the errors on the control and 50 ton/ha replicates. We derive the following mean soil Wrs (**Fig. S13)**.

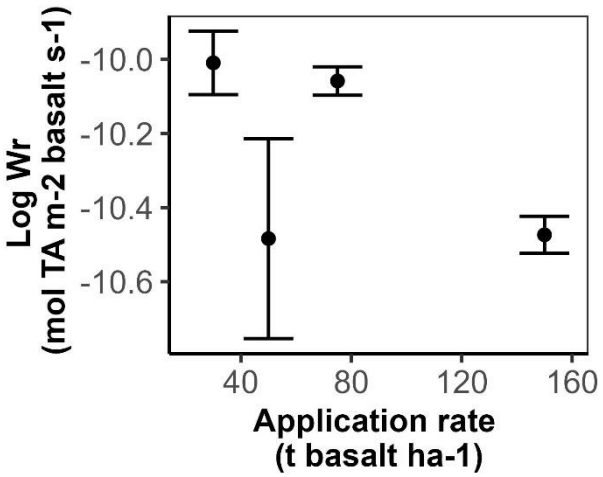

Fig. S13: Log Wr (mean +- standard error) of basalt based on the sum of alkalinity in all soil pools, the plant pool and the leachate pool. n=4 for the control and 50 t basalt ha^{-1} replicates. Note that the uncertainty for the Wr of the 30, 75 and 150 t ha^{-1} application rates equals the uncertainty of the control and is the same, yet to derive the log(se) for each application rates, the standard error transforms differently for each application rate as the formula Abs(Wr/standard error (Wr)*LN(10)) is used for log10 transforming uncertainties.

The order of the obtained weathering rates in **Fig. S13** is similar and even higher as the aggregated value from the slope approach (Log Wr = -11) obtained in the main manuscript. For individual application rates, the uncertainty is smaller than the in the slope approach due to larger standard errors of the regression in the regression approach.

S3.5 Soil organic C (calculated from loss on ignition) in function of basalt amendment.

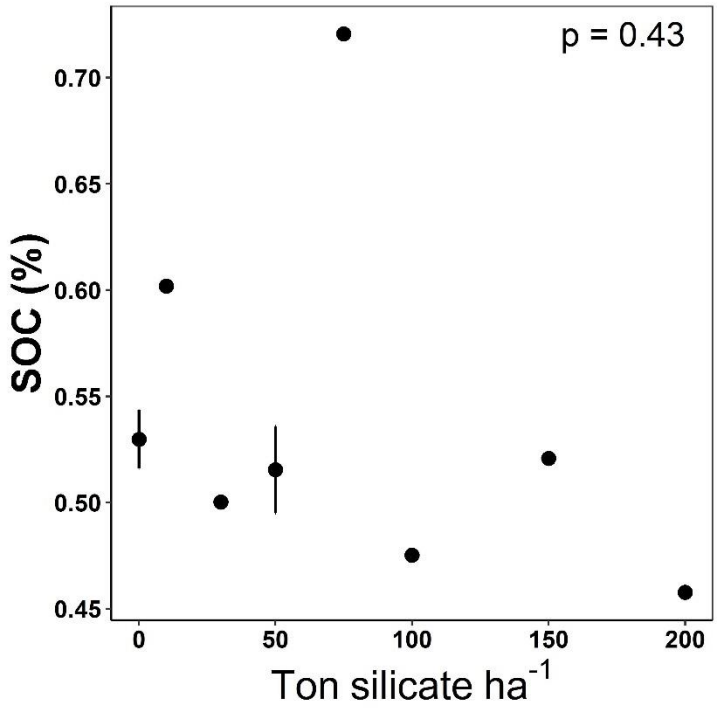

Fig. S14: SOC from loss on ignition (4 hours at 360°C) in function of basalt amendment, assuming a SOC/SOM ratio of 0.58. n=4 for the control soil and n=5 for the 50 t basalt ha^{-1} replicates.

S3.6 Si in soil pools

Si in the oxidizable pool of the top soil significantly increased with larger basalt amendment (**Fig. S15**).

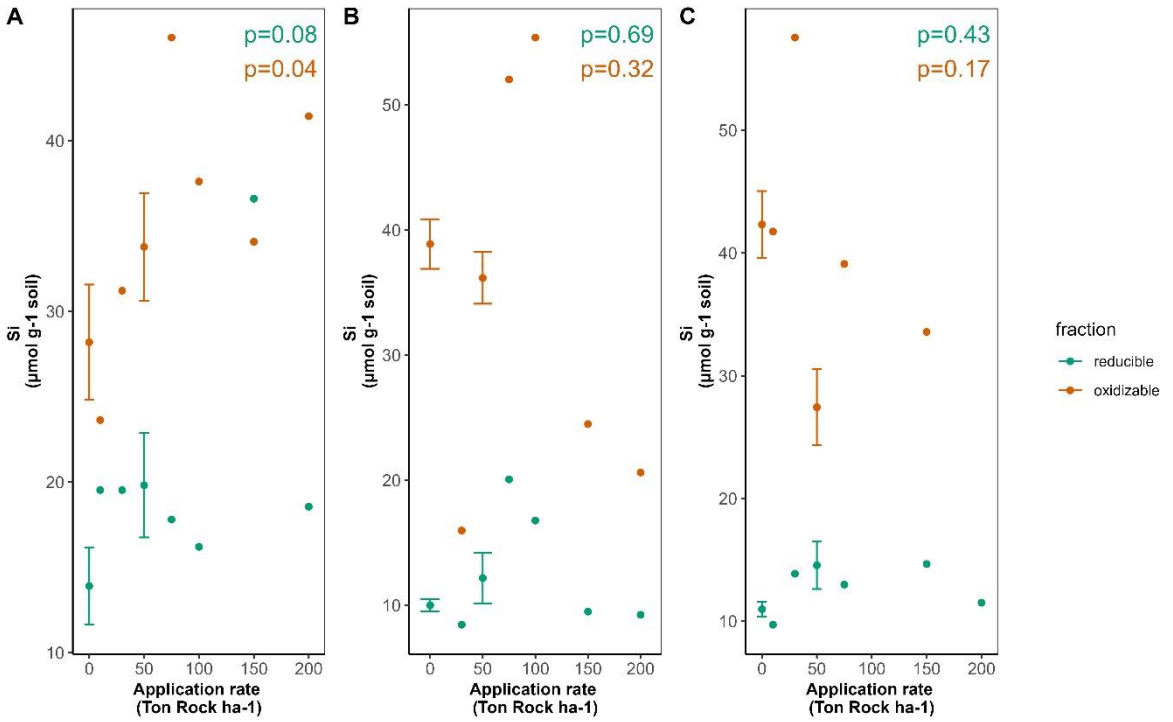

Fig. S15: Changes in Si in the reducible and oxidizable fraction after 100 days in the (A) 0-20 cm (B) 20-30 cm and (C) 30-50 cm soil layers. n = 4 for control and 50 t ha-1 replication. Dots and error bars represent averages and standard errors for each application rate.

S3.7 SIC measurement methods

SIC can be measured with several techniques, including calcimetry, techniques that rely on solid phase elemental C analysis, thermal carbonate decomposition (e.g. rock-eval) and carbonate extractions using acetic acid (Larkin et al., 2022; Manning & Renforth, 2013; Wattripont et al., 2019). Besides the carbonate extractions, we compare here with other methods.

SIC was quantified using four approaches: Decalcification without LOI pre-treatment, LOI+decalcification, calcimetry and carbonate extraction. The principle of the first method, the decalcification method is to estimate SIC as the difference between total soil carbon (TC) and soil organic carbon (SOC) (**Equation S1**). Soil TC was measured using an elemental CN analyzer (Flash 2000 CN Soil Analyser, Interscience, Louvain-la-Neuve, Belgium). The SOC was determined as the total C after degassing SIC by adding 10% HCl to each sample (acid destruction, followed by drying 1 day at 100°C). SIC was determined at each depth for each mesocosm and the average of six technical replicates is reported.

$$\text{Decalcification: SIC } [\%] = \left(\text{TC } \left[\frac{\text{gC}}{\text{gSoil}}\right] - \text{ SOC} \left[\frac{\text{gC}}{gsoil}\right]\right) * 100 \quad \text{(S1)}$$

As soils typically contain more SOC than SIC, SOC heterogeneity limits detection of small changes in SIC. We therefore also applied the LOI-decalcification method, which removes organic carbon prior to measuring SIC. Specifically, soil was first dried at 105°C and organic carbon was then removed by heating at 360°C for 4 hours in a muffle furnace (Nabertherm LE 6/11/R7). The temperature was limited to 360°C to avoid carbonate destruction (Dudhaiya et al., 2019). Organic carbon was calculated from the loss on ignition (LOI) assuming 58% C in soil organic matter (Van Bemmelen, 1890). The remaining carbon (TC_postCombustion) was determined after LOI using an elemental analyzer (Flash 2000 CN Soil Analyser, Interscience, Louvain-la-Neuve, Belgium). To correct for thermoresistant SOC that was not combusted in the muffle furnace, samples were acidified with 10% HCl, dried for 1 day at 100°C and the remaining C ($\text{SOC\_postcombustion}$) was measured. Finally, SOC and SIC were calculated as in **Equations S2 and S3**.

$$SIC[\%] = \left(\text{TC}_{\text{postCombustion}\left[\frac{\text{gC}}{\text{gSoil}}\right]} - \text{SOC}_{\text{postcombustion}\left[\frac{\text{gC}}{\text{gSoil}}\right]}\right) * 100 \quad \text{(S2)}$$

$$LOI + decalcification:$$

Third, calcimetry was used to estimate the carbonate content, using a calcimeter (Model 08.53, Royal Eijkelkamp, Giesbeek, The Netherlands). A calibration series of 2, 5, 10, 20, 100, 200 and 400 mg $CaCO_3$ was obtained by measuring the volume of CO_2 production after 7 mL of 4 M HCl was added and the substrate was shaken. Afterwards, this procedure was repeated with 3 g of dry soil and SIC was calculated as in **Equation S3.** For calcimetry, identical mesocosms were measured twice to decrease uncertainty of results.

$$SIC\ [\%] = \frac{\left(Callibration\ intercept\ [mL] + \ delta\ V_{CO2}[mL] * Callibration\ Slope\ \left[\frac{gCaCO3}{mL\ CO2}\right]\right) * \frac{12}{100}\left[\frac{gSIC}{g\ CaCO3}\right] * 100}{3\ [g\ soil]} \quad (S3)$$

$$Calcimetry:$$

The fourth approach for estimating changes in SIC content is through carbonate extractions, using a back-calculation of SIC based on extracted carbonate-cations. After extraction of the exchangeable soil pool, in the second extraction step of the sequential extractions (acetate leaching) base cations and Fe were analyzed. Divalent cations (Ca, Mg and Fe) have a 1:1 ratio with pedogenic carbonates, while for K, a 2:1 K:SIC ratio was utilized. After multiplication with extraction buffer volume added to 1 g of soil (8 mL), the equivalent SIC% in the soil sample was calculated as in **Equation S4**.

$$SIC[\%] = \frac{\left((Ca + Mg + Fe)\left[\frac{mol}{L}\right] + \left(\frac{K}{2}\right)\left[\frac{mol}{L}\right]\right) * Extract\ Volume\ [L] * 12\left[\frac{gSIC}{mol\ SIC}\right] * 100}{Soil\ mass\ [g\ soil]} \quad (S4)$$

$Carbonate\ extraction$:

Last, we want to emphasize that only experimental samples and no standards were tested using these methods as the goal of this comparison was to investigate whether a signal could be detected after basalt amendment, rather than identifying the optimal method for SIC measurement.

Comparison of SIC measuring techniques showed that the decalcification method gave significantly higher SIC values than calcimetry, LOI-decalcification and carbonate extractions ($p<0.01$) (**Fig. S16**). We only detected a significantly increase in SIC with higher basalt amendment using carbonate extractions (**Fig. S16D)**. Variation differed strongly between methods, with SIC derived from LOI-decalcification showing standard errors that were 10 times than those for SIC derived from carbonate extractions (**Fig. 16C and D).**

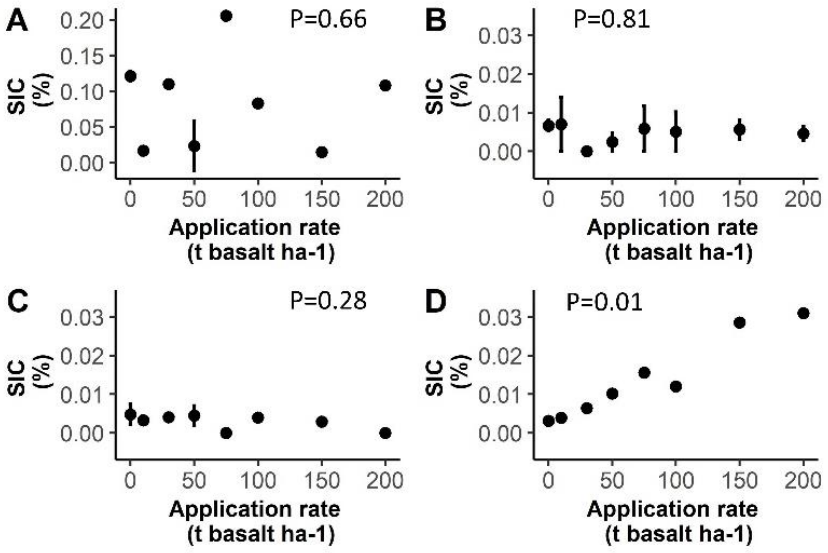

Fig. S16: The relationship between SIC in top soil (0-20cm) and basalt amendment, with SIC measured with four different methods: (A) The decalcification method (B) Calcimetry (C) LOI-decalcification and (D) carbonate extractions. These analyses were done on soil sampled after 101 days. Dots and error bars represent averages and standard errors for technical replicates in panel B. Only for two application rates (0 and 50 ton basalt ha^{-1}), replicates per application rate were established and error bars are shown. p-values of the basalt effect are indicated in the figure. Error bars in panel D are smaller than the dot symbols. Note that the y-axis limit of panel A exceeds 0.20% as results heterogeneity was large, while the y axes for other panels are limited to <0.04%. n=5 for the control soil and 50 t basalt ha^{-1} replicates in all panels except for in panel B, where twice as much measurements occurred so that n= 10 for the control soil and 50 t basalt ha^{-1} replicates and n=2 for other application rates.

Acetate leaching (=carbonate extractions) was thus the only method that detected increases in SIC after basalt amendment (**Fig. S6D).** When we correct the increase observed in **Fig. 16D** with carbonates added with the basalt feedstock (**Fig. S18**), we observe a decrease in top soil carbonates after 101 days (due to a decrease in carbonate-Ca). Corrected for feedstock carbonate, top soil (0-20 cm) SIC thus decreased in time with larger basalt amendment. Across the entire soil profile, we observe a decrease in carbonate base cation charges (see main text). This shows that considering feedstock carbonates is key in quantifying small SIC changes after rock amendment. Moreover, correction for feedstock carbonates may be especially relevant for rock feedstocks high in carbonates such as wollastonite skarn.

S3.8 Carbonate saturation states

The saturation states of CaCO3 and dolomite were simulated using PHREEQC for every application rate in time in **Fig. S17**.

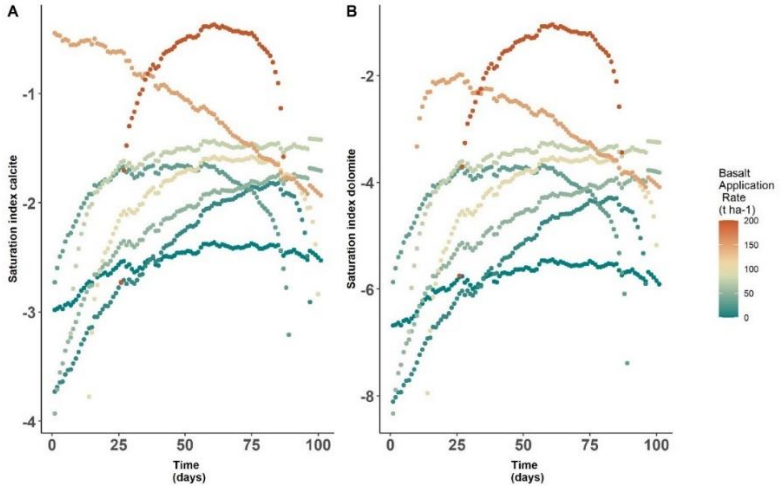

Fig. S17: PHREEQC calculated Log saturation index of (A) Calcite and (B) Dolomite in function of time for a range of basalt applications.

S3.9 The necessity to correct for feedstock addition to quantify weathering rates.

As mentioned in the discussion, increases in weathered base cations in soil pool should be corrected for amendment increases because of addition of already weathered bases with rock feedstock. The relative importance of feedstock addition relative to the total base cation increase observed after 101 days is shown in **Fig. S18**.

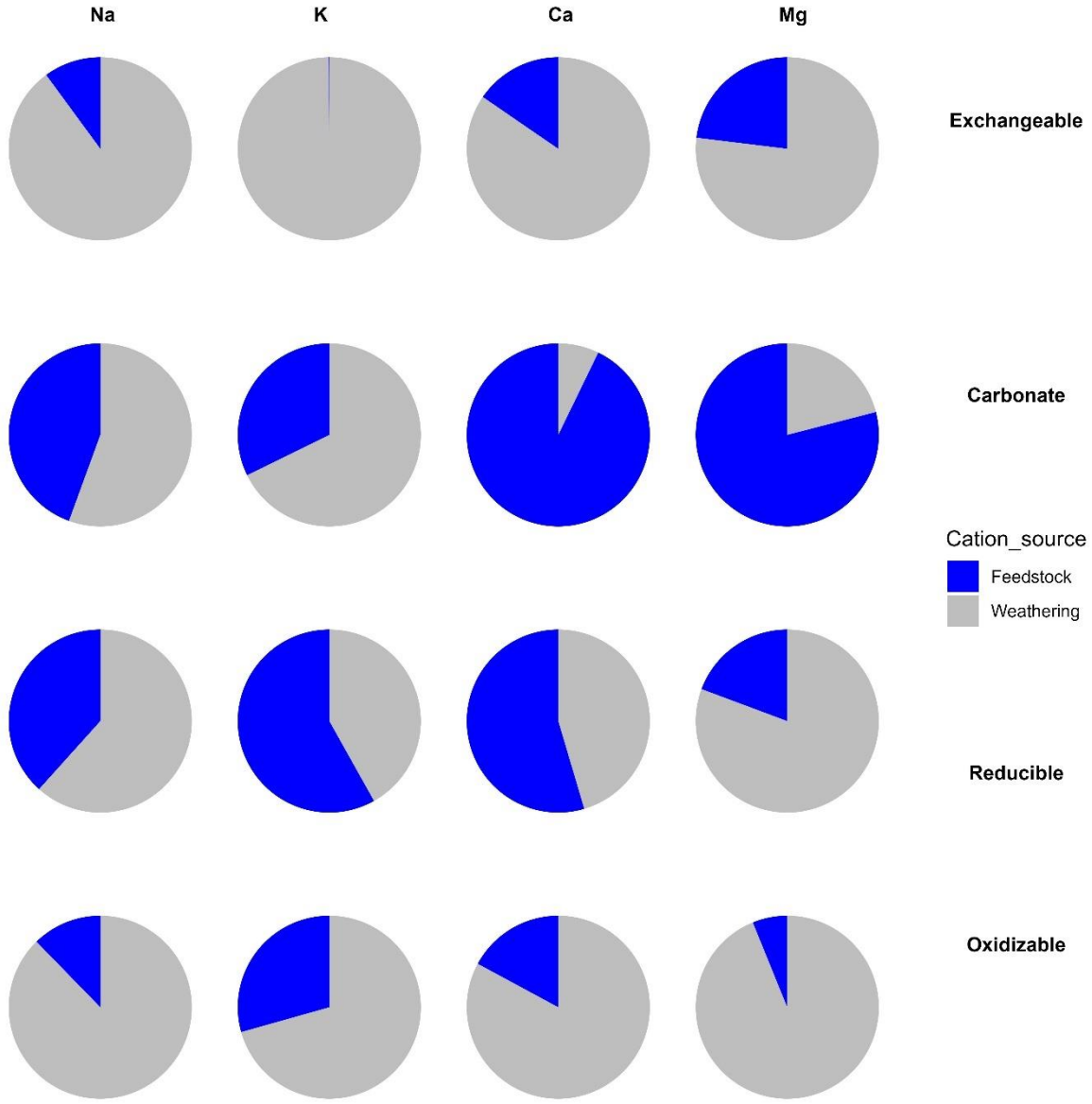

Fig. S18: Necessity to correct for pre-weathered rock feedstock. Relative contribution of feedstock addition and rock weathering to increases in basalt amended relative to control soils of Na, K, Mg and Ca in the exchangeable, carbonate, reducible and oxidizable soil pools. Averages of all basalt application rates were visualized here.

S3.10 Raw extraction data plots (unnormalized for control soil)

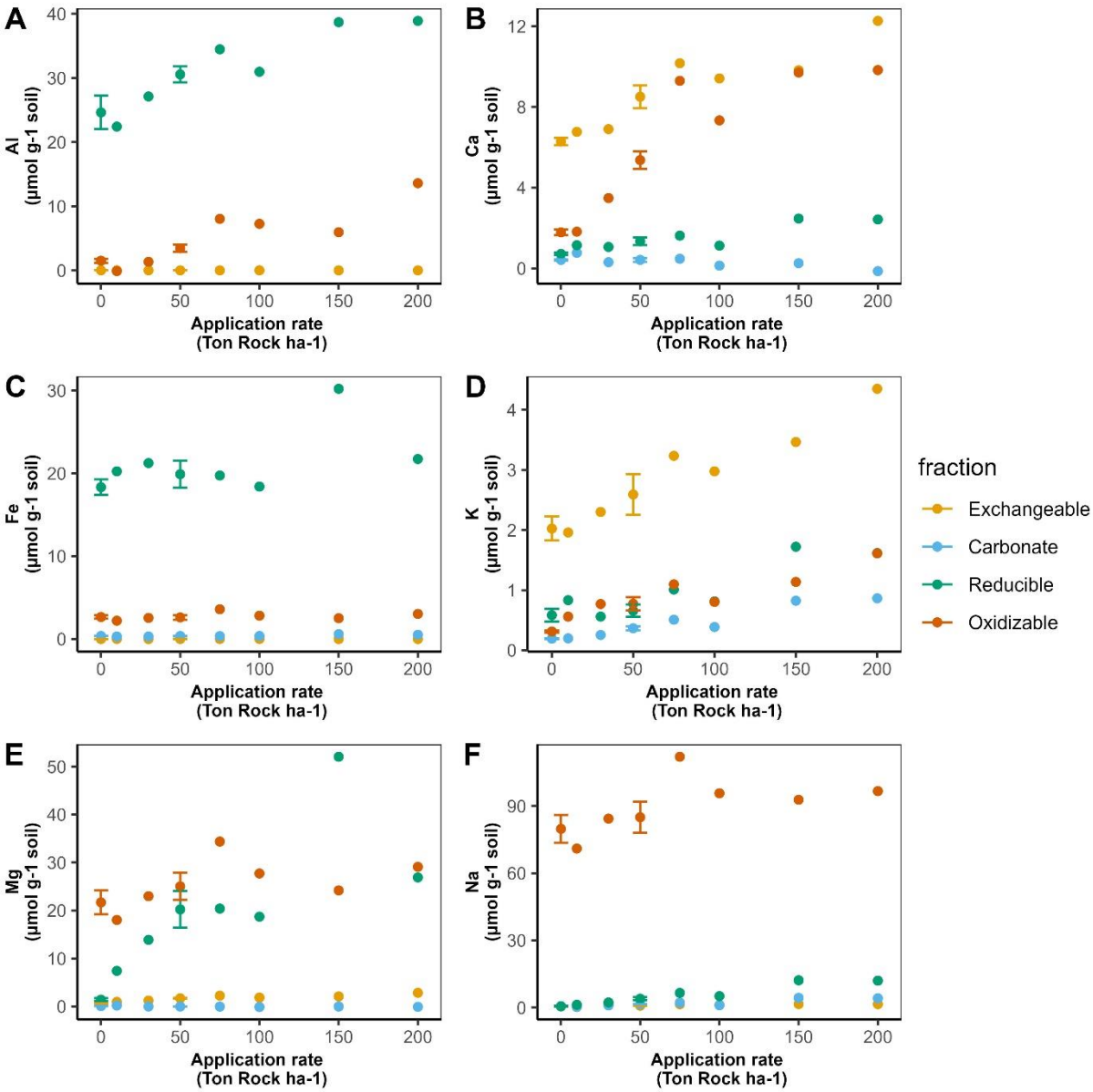

Fig. S19: Change in Top soil (0-20 cm) elements, 100 days after basalt amendment ((corrected as in **Equation 7**) as a function of rock application rate for (A) Al (B) Ca (C) Fe (D) K (E) Mg and (F) Na for four different soil pools, unnormalized for control soils. n>=4 for every fraction for control and n=4 for the 50 t ha-1 replication. Dots and error bars represent averages and standard errors. Note that y-axes absolute values differ for subplots to visualize smaller changes for certain elements.

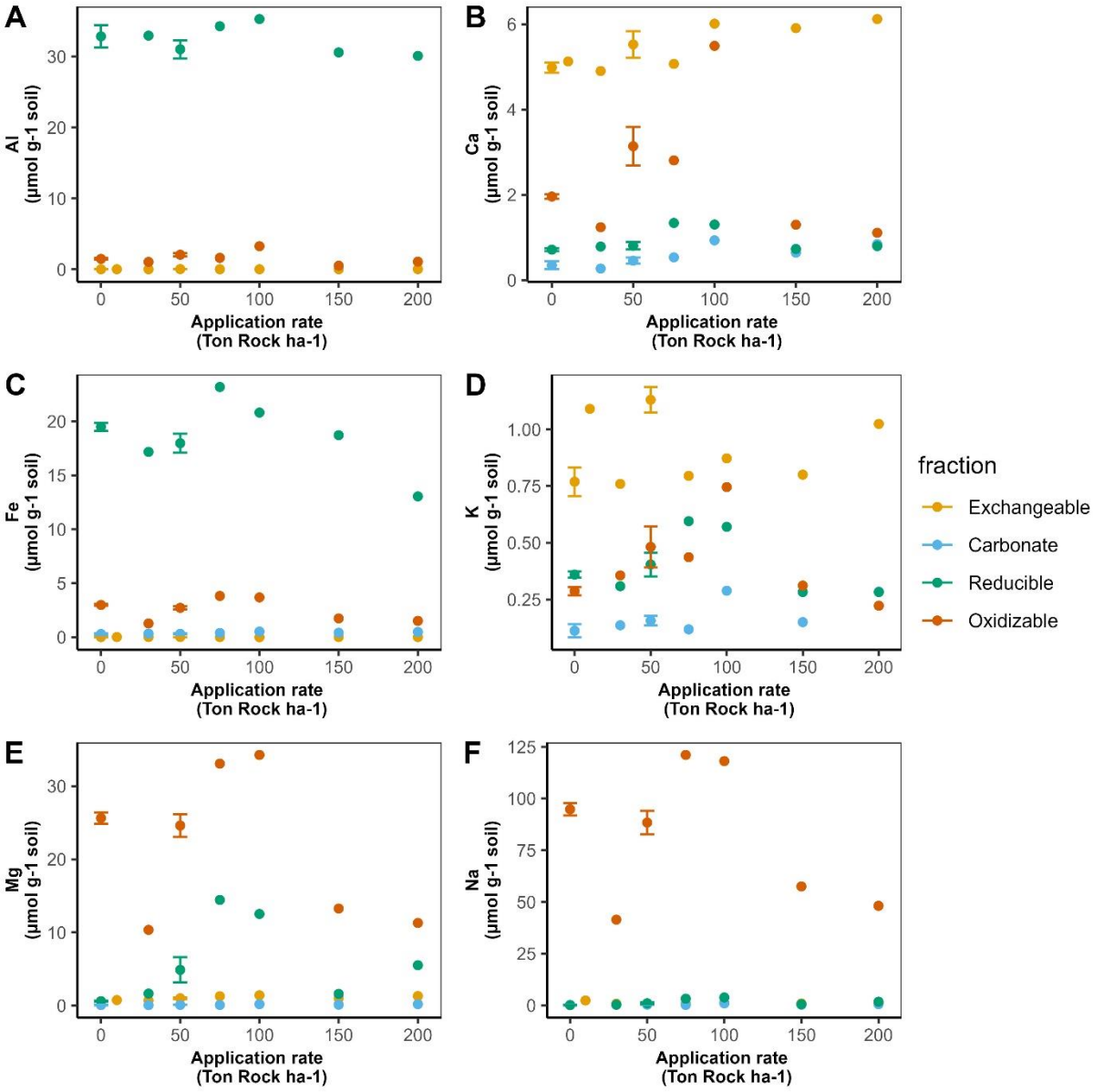

Fig. S20: Change in soil (20-30 cm) elements, 100 days after basalt amendment as a function of rock application rate for (A) Al (B) Ca (C) Fe (D) K (E) Mg and (F) Na for four different soil pools, unnormalized for control soils. n = 4 for control and 50 t ha-1 replication. Dots and error bars represent averages and standard errors. Note that y-axes absolute values differ for subplots to visualize smaller changes for certain elements.

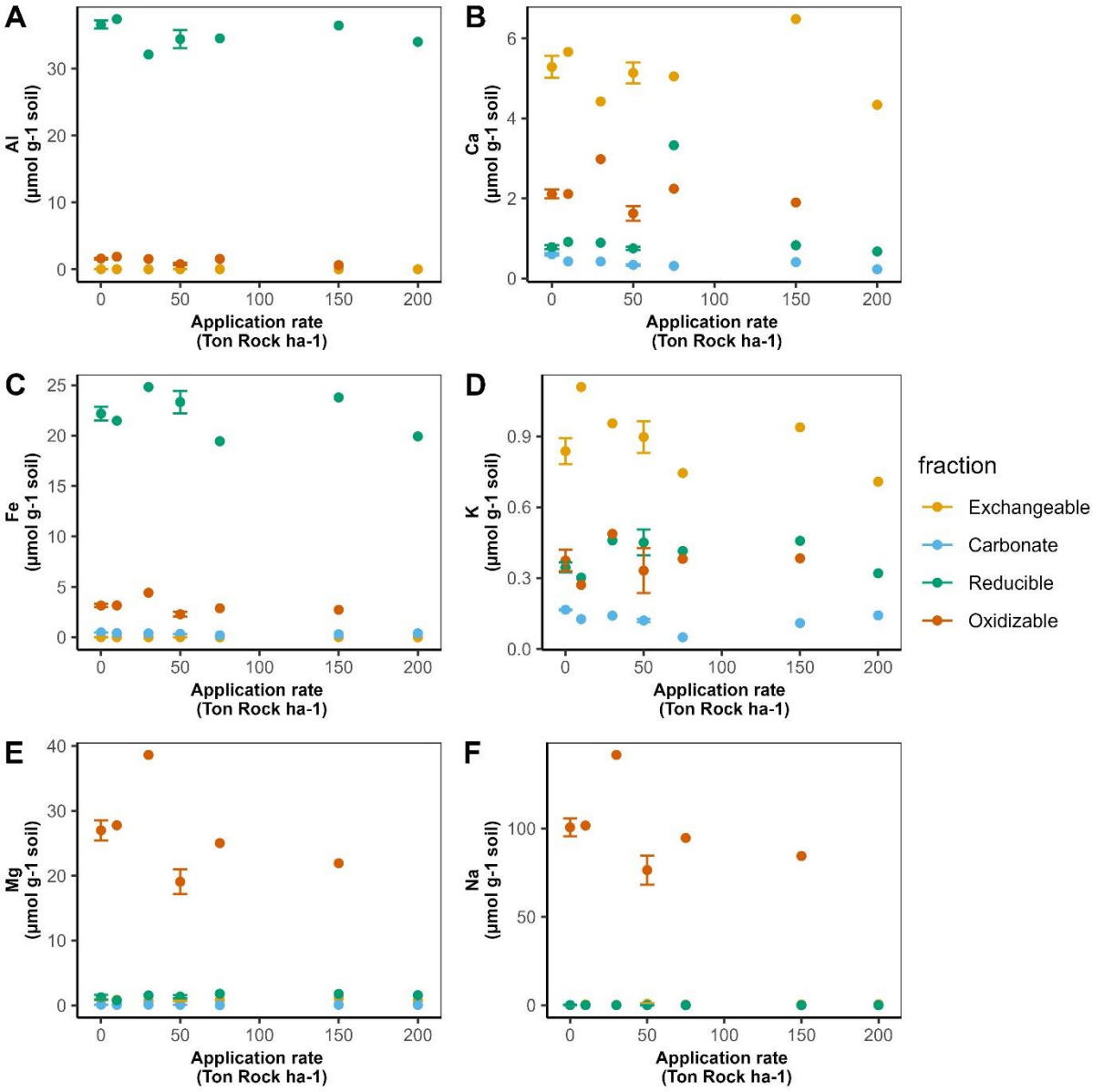

Fig. S21: Change in soil (30-50 cm) elements, 100 days after basalt amendment as a function of rock application rate for (A) Al (B) Ca (C) Fe (D) K (E) Mg and (F) Na for four different soil pools, unnormalized for control soils. n = 4 for control and 50 t ha-1 replication. Dots and error bars represent averages and standard errors. Note that y-axes absolute values differ for subplots to visualize smaller changes for certain elements.

S3.11 Linear versus logarithmic regression approach

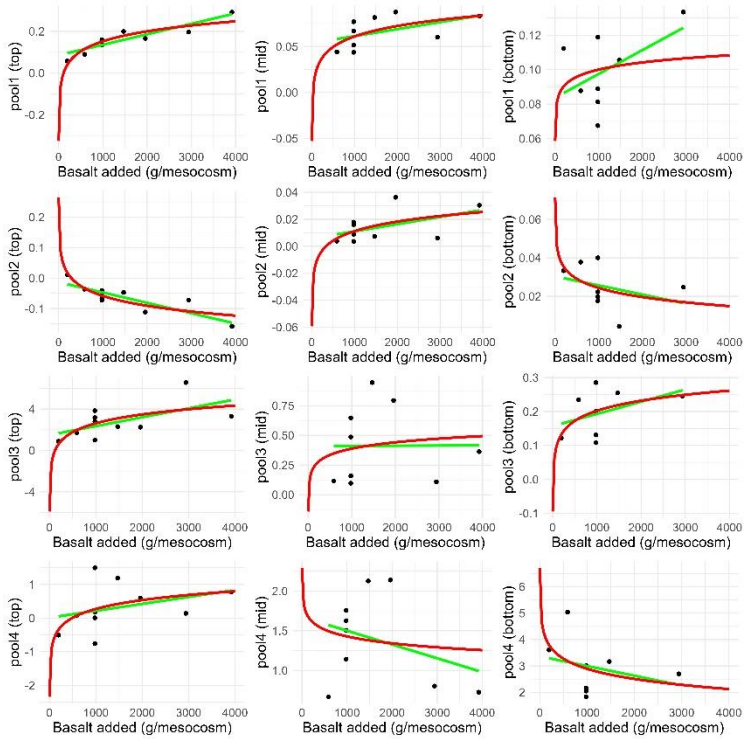

Fig. S22: linear (green) versus logarithmic (red) regressions of the TA change relative to the control in function of added basalt. Pool 1= exchangeable, pool 2= carbonates, pool 3= reducible, pool 4= oxidizable. "Top"= 0-20 cm depth, "Mid" = 20-30 cm, "bottom" = 30-50 cm.

Table S5: R^2, AIC and p value of linear and logarithmic regressions shown in Supplementary Figure 23.

Pool	Depth	R2_Linear	AIC_Linear	P_Linear	R2_Log	AIC_Log	P_Log
pool1	top	**0.786**	**-38.316**	**0.000391**	**0.820**	**-40.060**	**0.000192**
pool1	mid	0.137	-45.302	0.175000	0.253	-46.602	0.095300
pool1	bottom	0.143	-36.038	0.192000	-0.114	-33.944	0.613000
pool2	top	**0.691**	**-41.341**	**0.001760**	**0.718**	**-42.260**	**0.001200**
pool2	mid	0.139	-51.872	0.174000	0.173	-52.234	0.146000
pool2	bottom	-0.041	-44.325	0.427000	0.067	-45.197	0.267000
pool3	top	0.277	38.840	0.068000	**0.328**	**38.107**	**0.048700**
pool3	mid	-0.143	10.140	0.993000	-0.119	9.949	0.710000

Pool	Depth	R2_Linear	AIC_Linear	P_Linear	R2_Log	AIC_Log	P_Log
pool3	bottom	0.046	-16.872	0.291000	0.107	-17.401	0.224000
pool4	top	0.000	25.141	0.346000	0.106	24.024	0.188000
pool4	mid	-0.016	19.575	0.380000	-0.123	20.478	0.735000
pool4	bottom	-0.070	27.579	0.489000	0.030	26.793	0.312000

S3.12 Mass balance element changes in fraction relative to elements in basalt

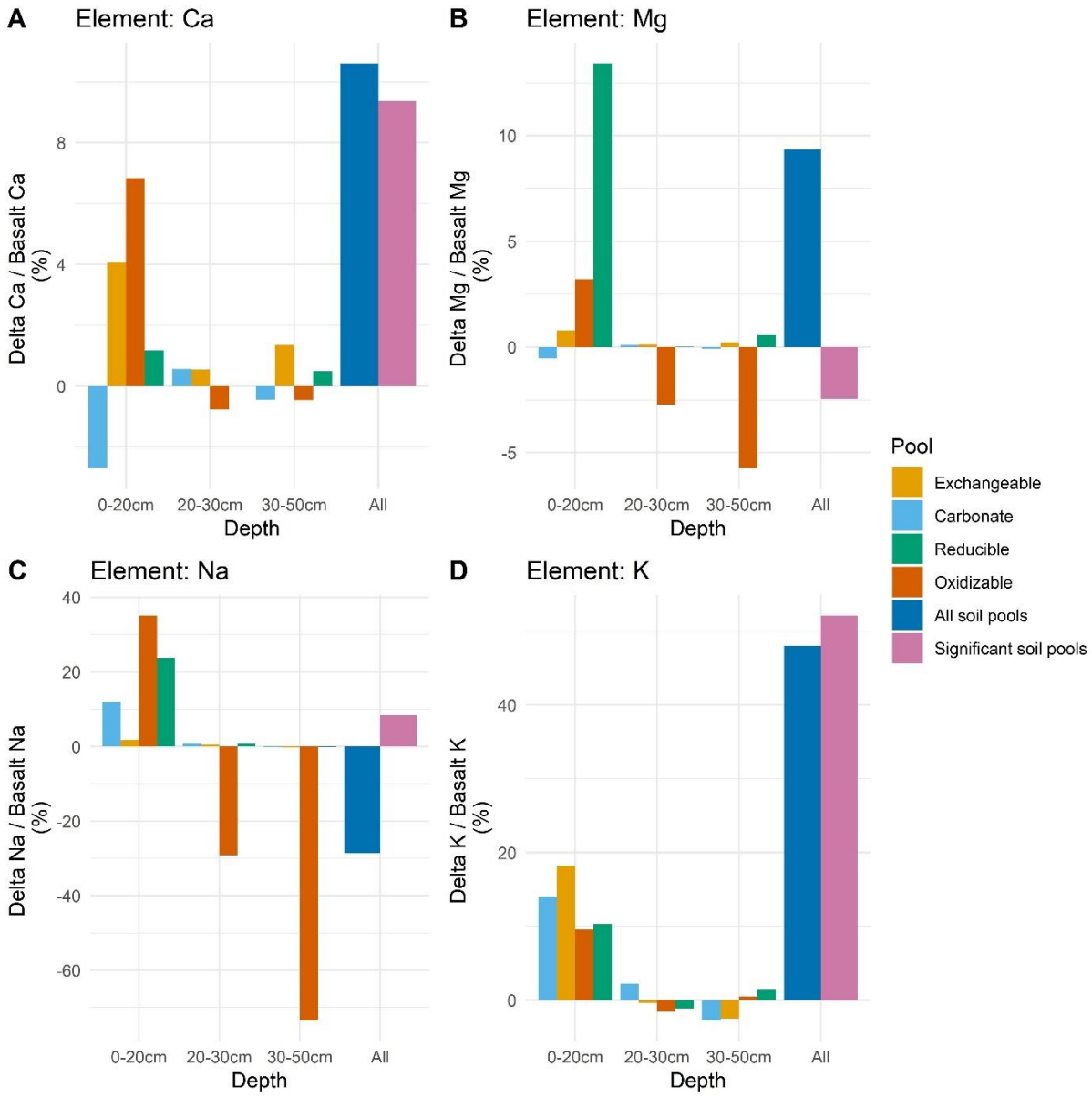

Fig. S23: Mass fraction of weathered basalt for the four base cations.

The contribution of base cations in the topsoil pore water was minor in comparison with the slope observed in solid soil pools (⇔ Fig. 6 main text with **Fig. S24**). For Ca and Mg for example, we find an increase in pore waters of 0.76 and 0.33 µmol/g basalt (negligible relative to the increase observed in solid soil pools, that were in the 100s of µmol/g basalt for both Ca and Mg).

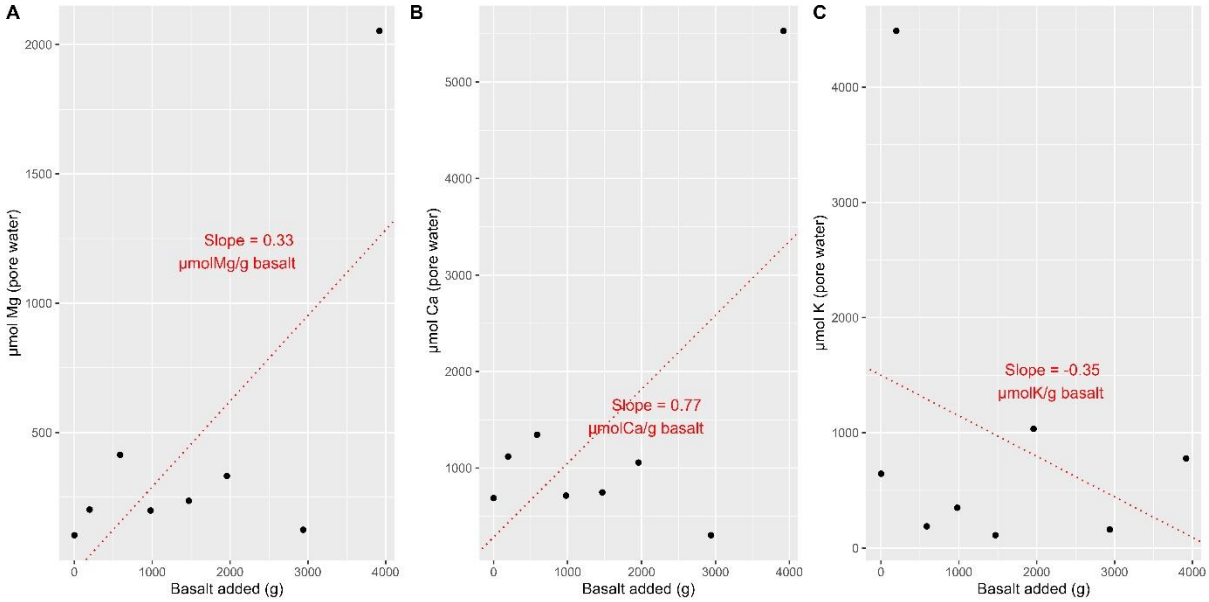

Fig. S24: Elemental increase base cations in pore water (0-20cm) in function of basalt amended (g) for (A) Mg (B) Ca (C) K. This figure shows the mean of all measured pore water Mg, Ca and K (n= 66, 66 and 55 respectively).